Article

Compositional Design of Soft Magnetic High Entropy Alloys by Minimizing Magnetostriction Coefficient in $(Fe_{0.3}Co_{0.5}Ni_{0.2})_{100-x}(Al_{1/3}Si_{2/3})_x$ System

Yong Zhang [1,*], **Min Zhang** [1], **Dongyue Li** [1], **Tingting Zuo** [2], **Kaixuan Zhou** [3], **Michael C. Gao** [4,5], **Baoru Sun** [3] and **Tongde Shen** [3]

[1] The State Key Laboratory of Advanced Metals and Materials, University of Science and Technology Beijing, Xueyuan Road 30, Beijing 100083, China; zhangminw925@163.com (M.Z.); lidongyue03@163.com (D.L.)
[2] Interdisciplinary Research Center, Institute of Electrical Engineering, Chinese Academy of Sciences, Beijing 100190, China; zuott1986.520@163.com
[3] State Key Laboratory of Metastable Materials Science and Technology, Yanshan University, Qinhuangdao 066004, China; zkx@stumail.ysu.edu.cn (K.Z.); sunbaoru@ysu.edu.cn (B.S.); tdshen@ysu.edu.cn (T.S.)
[4] National Energy Technology Laboratory, Albany, OR 97321, USA; michael.gao@netl.doe.gov
[5] Leidos Research Support Team, P.O. Box 10940, Pittsburgh, PA 15236, USA
* Correspondence: drzhangy@ustb.edu.cn; Tel.: +86-186-0008-0235

check for updates

Abstract: Developing cost-effective soft magnetic alloys with excellent mechanical properties is very important to energy-saving industries. This study investigated the magnetic and mechanical properties of a series of $(Fe_{0.3}Co_{0.5}Ni_{0.2})_{100-x}(Al_{1/3}Si_{2/3})_x$ high-entropy alloys (HEAs) (x = 0, 5, 10, 15, and 25) at room temperature. The $Fe_{0.3}Co_{0.5}Ni_{0.2}$ base alloy composition was chosen since it has very the smallest saturation magnetostriction coefficient. It was found that the $(Fe_{0.3}Co_{0.5}Ni_{0.2})_{95}(Al_{1/3}Si_{2/3})_5$ alloy maintains a simple face-centered cubic (FCC) solid solution structure in the states of as-cast, cold-rolled, and after annealing at 1000 °C. The alloy after annealing exhibits a tensile yield strength of 235 MPa, ultimate tensile strength of 572 MPa, an elongation of 38%, a saturation magnetization (Ms) of 1.49 T, and a coercivity of 96 A/m. The alloy not only demonstrates an optimal combination of soft magnetic and mechanical properties, it also shows advantages of easy fabrication and processing and high thermal stability over silicon steel and amorphous soft magnetic materials. Therefore, the alloy of $(Fe_{0.3}Co_{0.5}Ni_{0.2})_{95}(Al_{1/3}Si_{2/3})_5$ holds good potential as next-generation soft magnets for wide-range industrial applications.

Keywords: high-entropy alloy; soft magnetic properties; mechanical properties; saturation magnetostriction coefficient; face-centered cubic (FCC) structure

1. Introduction

Contrasted to the traditional alloy design concept that is based on one or two major elements, high-entropy alloys (HEAs) usually contain four or more major elements, and the content of each major element is above 5 at% [1–10]. The high configurational entropy of the HEAs tends to promote forming the solid solution phases with the face-centered cubic (FCC) [11–15], body-centered cubic (BCC) [16,17], and hexagonal-close-packed (HCP) structures [18–20], as well as dual solid-solution phases [21–23]. The composition of HEAs is generally near the center of the multi-component phase diagram, and hence it is difficult to distinguish the solvent from the solute. The following 5 characteristics are typically and have been verified for the HEAs [4,24,25]:

(1). high thermal stability and resistance to heat softening;
(2). easier to break the tradeoff between strength and ductility;
(3). very low stacking-fault energy;
(4). high irradiation resistance;
(5). high corrosion resistance.

Consequently, HEAs show promising potentials for wide ranges of industrial applications and the HEA concept is considered to be one of the three major breakthroughs in alloying theory [3].

To date considerable research efforts on HEAs focus on their microstructures and mechanical properties [26–31] while there is rising interest in developing high-entropy soft magnetic materials [32–40]. Magnetic materials play a fundamental role in transformers, motors, electromagnets, and other power industries [41]. Common soft magnetic alloys include silicon steel, ferrite, iron-nickel alloys, and bulk metallic glasses. However, to date many challenges still remain for energy-saving and high-performance applications. For example, it is time-consuming to produce and process silicon-steels [42]. Ferrite has low magnetization, iron-nickel alloy has low resistivity, and bulk metallic glass are inherently brittle and are also limited to small size [43,44]. Recent studies have shown that FeCoNiAlSi-based and FeCoNiMnAl-based HEAs exhibit high saturation magnetization which open up new research directions of soft magnetic materials [45]. However, the coercivity of HEAs is a bit high, for example, the coercivity of $FeCoNi(Al,Si)_{0.2}$ alloy is 1400 A/m [46]. It is known that the magnetic properties of HEAs are sensitive to the alloy system and the composition, the phase crystal structures, and the microstructure.

In terms of soft magnetic materials, the most important characteristic is high permeability, high saturation induction, low core loss and low coercivity. In this study, ferromagnetic elements Fe, Co, and Ni were selected as the main constituents of the alloy system [47]. The base alloy composition $Fe_{0.3}Co_{0.5}Ni_{0.2}$ was chosen since the alloy has a close-to-zero saturation magnetostriction coefficient (λs) as shown in the Co-Fe-Ni ternary system (Figure 1). To balance soft magnetic and mechanical properties, Al and Si in small amount was added to $Fe_{0.3}Co_{0.5}Ni_{0.2}$, and the resulting materials properties of the $(Fe_{0.3}Co_{0.5}Ni_{0.2})_{100-X}(Al_{1/3}Si_{2/3})_X$ (X = 0, 5, 10, 15, and 25) high entropy alloys were studied systematically. It was found that the $(Fe_{0.3}Co_{0.5}Ni_{0.2})_{95}(Al_{1/3}Si_{2/3})_5$ alloy exhibits excellent soft magnetic properties. The alloy has small coercivity of 96 A/m, and the saturation magnetic induction (Bs) and the saturation magnetization (Ms) reached 1.55 T and 1.49 T, respectively. The alloy in the as-cast state also shows an excellent tensile elongation up to 25% and a yield stress of 122 MPa at room temperature.
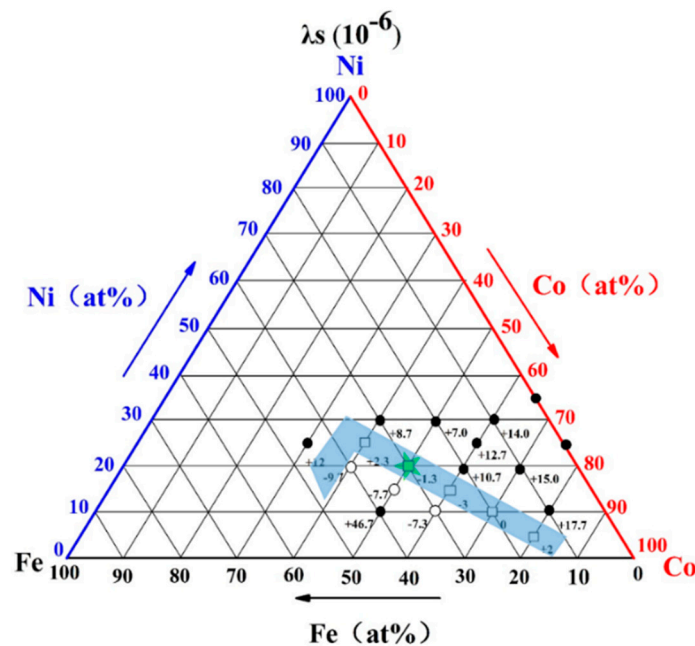
Figure 1. The saturation magnetostriction (λs) of the Co-Fe-Ni bulk ternary alloys at room temperature.

2. Materials and Methods

2.1. Alloys Preparation

Al, Co, Cr, Fe, and Ni elements with purities of greater than 99.5 wt.% were used to prepare $(Fe_{0.3}Co_{0.5}Ni_{0.2})_{100-X}(Al_{1/3}Si_{2/3})_X$ alloys ingots using vacuum arc melting (VAM) and magnetic levitation melting (MLM). The alloys were remelted five times in order to improve the chemical homogeneity. The ingot of the maglev melted alloy is cut into a plate with a thickness of 6 mm. Then the plate was cold rolled to a thickness of 1 mm (i.e., thickness reduction of 83%) by multi-pass rolling, with 0.5 mm reduction for each step. Subsequent annealing heat treatment was performed at 1000 °C for 2 h followed by water quenching or furnace cooling.

2.2. Structural Characterization and Performance Experiments

The crystal structures of the ingots were measured by a Smart Lab X-ray diffractometer (Bruker D8, Karlsruhe, Germany), using Cu-Kα radiation. The electron backscatter diffraction (EBSD) was carried out by a field emission scanning electron microscope (ZEISS SUPRA 55, Jena, Germany). Room temperature compression and tensile tests were conducted on a CMT Model 4305 Universal Electronic Tester with a strain rate of 1×10^{-3} min^{-1}. A hysteresis loop and hysteresis loss curve were obtained by PPMS (physical property measurement system) and VSM (Vibrating Sample Magnetometer) at room temperature. The four-point method was used for measuring the electrical resistance.

3. Results

Figure 2 shows the XRD profiles of $(Fe_{0.3}Co_{0.5}Ni_{0.2})_{100-X}(Al_{1/3}Si_{2/3})_X$ HEAs, (X = 0, 5, 10, 15, and 25). When X = 0, 5, and 10, the alloys possess a simple FCC structure. When X reaches 15, BCC phase appears and the alloy exhibits an FCC + BCC dual-phase structure. When the $(Al_{1/3}Si_{2/3})$ content increases to 25, the FCC phase disappears and only BCC phase was detected. Al has a much larger atomic radius than the transition metal elements of the alloys and it is known as a potent BCC phase stabilizer in steels. Figure 3 shows the hysteresis loops of the $(Fe_{0.3}Co_{0.5}Ni_{0.2})_{100-X}(Al_{1/3}Si_{2/3})_X$ series alloys at room temperature. The saturation magnetization of these alloys decreases gradually from 168.06 Am^2/kg to 116.48 Am^2/kg with increasing $(Al_{1/3}Si_{2/3})$ contents.
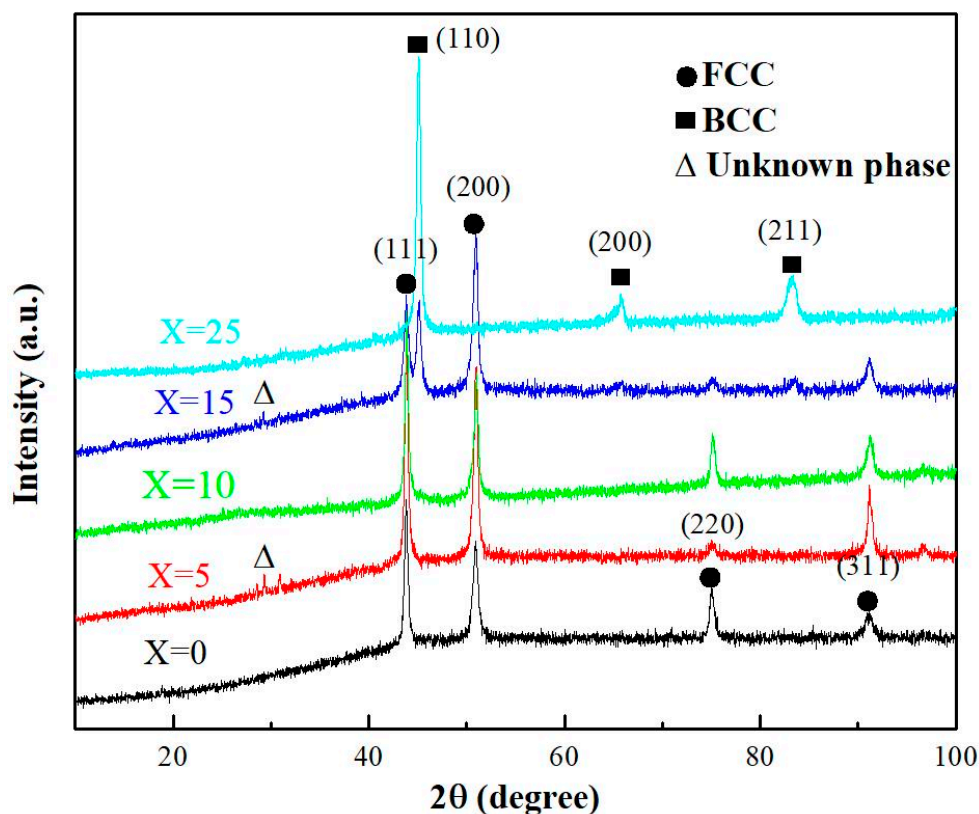
Figure 2. X-ray diffraction (XRD) patterns of $(Fe_{0.3}Co_{0.5}Ni_{0.2})_{100-X}(Al_{1/3}Si_{2/3})_X$ high-entropy alloys (HEAs) prepared using arc melting.
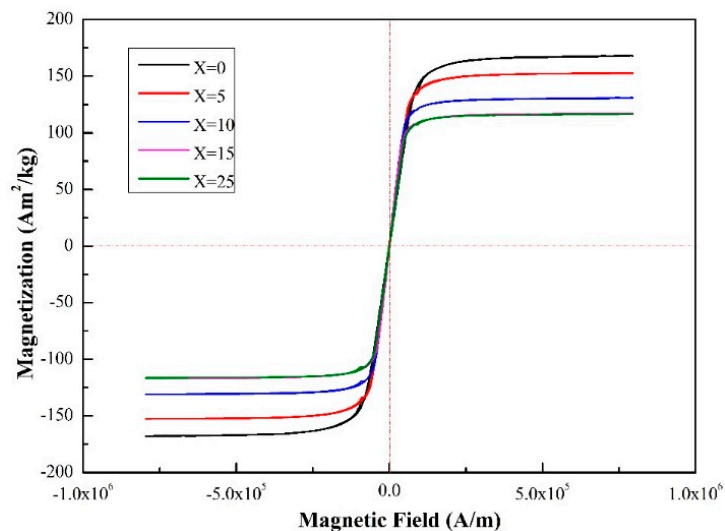

Figure 3. The hysteresis loops of $(Fe_{0.3}Co_{0.5}Ni_{0.2})_{100-X}(Al_{1/3}Si_{2/3})_X$ HEAs at room temperature.

The variation of the coercivity (Hc) and saturation magnetization (Ms) are shown in Figure 4. When X ≤ 10, the alloys maintain the FCC structure, and the coercivity increases with increasing Al and Si contents, increasing from 888 A/m to 1194 A/m. With higher Al and Si contents, the alloys become BCC dominant, and the Hc drops to 921 A/m when X = 15 but increases to 990 A/m when X = 25. Within a specific crystal structure, increasing Al and Si contents increase the atomic size difference and hence lattice distortion and coercivity.
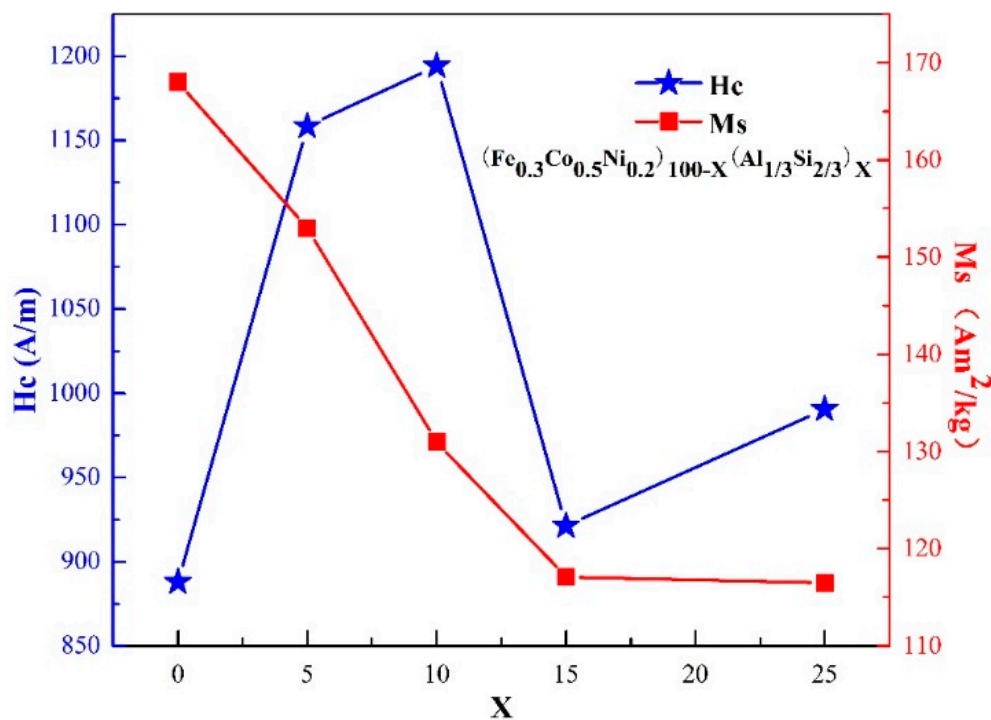
Figure 4. The variation of coercivity and saturation magnetization of $(Fe_{0.3}Co_{0.5}Ni_{0.2})_{100-X}(Al_{1/3}Si_{2/3})_X$ HEAs as a function of Al and Si contents.

The compression stress–strain behavior of $(Fe_{0.3}Co_{0.5}Ni_{0.2})_{100-X}(Al_{1/3}Si_{2/3})_X$ alloys is shown in Figure 5, and the corresponding yield stress and plastic strain are summarized in Table 1. In general, the yield stress of the alloys increases with increasing the $(Al_{1/3}Si_{2/3})$ content. When X = 5, the alloy maintains good plasticity with certain work hardening ability, and no fracture occurred during compression test. When X $\geq$ 15, the yield stress increases rapidly with a large reduction in plasticity.
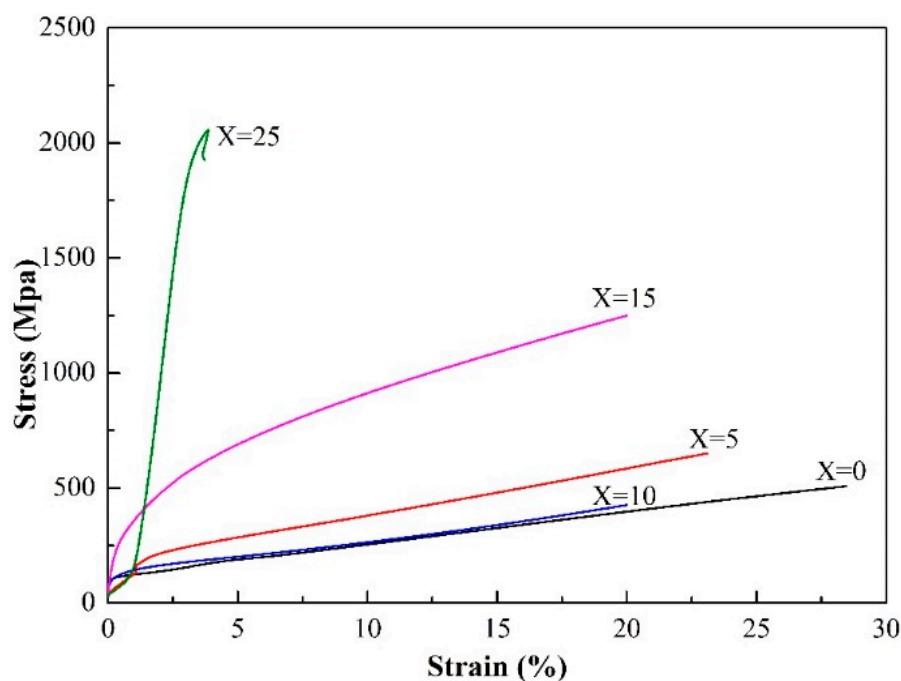

Figure 5. The compressive stress-strain curves of $(Fe_{0.3}Co_{0.5}Ni_{0.2})_{100-X}(Al_{1/3}Si_{2/3})_X$ HEAs at room temperature.

Table 1. The magnetic properties and compression behavior of $(Fe_{0.3}Co_{0.5}Ni_{0.2})_{100-X}(Al_{1/3}Si_{2/3})_X$ high entropy alloys at room temperature.

Alloys	Hc (A/m)	Ms (Am²/kg)	$\sigma_{0.2}$ (MPa)	σ_{max} (MPa)	ε_p (%)
X = 0	887.93	168.06	96	-	>20
X = 5	1158.37	153.45	122	-	>20
X = 10	1194.29	130.97	116	-	>20
X = 15	921.25	117.10	243	-	>20
X = 25	990.48	116.48	1445	2050	2.71

The variation of mechanical properties is attributed to the different phase structures and microstructures. Dissolution of Al and Si in the FCC lattice of transition metals of Fe, Co, and Ni causes severe lattice distortion, contributing to pronounced solid solution strengthening. However, excessive addition of Al and Si promotes the formation of BCC phase, and the strength of the alloy increases rapidly at the cost of significantly reduced plasticity. Similar trend on the effect of Al contents on the phase stability and mechanical properties of high entropy alloys is reported by Tang et al [48].

For industrial applications, it is necessary for HEAs to possess not only good soft magnetic properties, but also acceptable plastic deformation ability. The newly-designed $(Fe_{0.3}Co_{0.5}Ni_{0.2})_{95}(Al_{1/3}Si_{2/3})_5$ alloy in the present study has shown good potential for industrial application as high-performance soft magents. The saturation magnetization of the alloy reaches 153.45 Am²/kg and the resistivity is about 60.3 μΩ·cm. Besides, it also shows satisfactory ductility. A comprehensive characterization of the aloy is presented in the following sections.

Figure 6 shows the macroscopic appearance of $(Fe_{0.3}Co_{0.5}Ni_{0.2})_{95}(Al_{1/3}Si_{2/3})_5$ alloy by vacuum magnetic suspension melting and the sheet after cold-rolled. Figure 7 shows the X-ray diffraction pattern of the alloy in the as-cast, cold-rolled, water quenching, and furnace cooling states after heat treatment. A simple FCC structure can be clearly identified in all states while a small peak at around 30 degrees appears in the as-cast and furnace-cooled states.

Figure 6. The macroscopic appearance: (**a**) $(Fe_{0.3}Co_{0.5}Ni_{0.2})_{95}(Al_{1/3}Si_{2/3})_5$ alloy ingot prepared by maglev melting, (**b**) cold-rolled sheet.

Figure 8 presents the EBSD images of the $(Fe_{0.3}Co_{0.5}Ni_{0.2})_{95}(Al_{1/3}Si_{2/3})_5$ alloy in different conditions. The as-cast (Figure 8a) alloy shows a coarse column grain microstructure with the column width of ~1000 μm. After cold-rolling (83% thickness reduction), the grains are significantly elongated (Figure 8b). Annealing at 1000 °C caused complete recrystallization and the resulting grain sizes were significantly smaller than in the as-cast and cold-rolled states (Figure 8c,d). Annealing also introduced the formation of a large number of annealing twins but there was no preferred grain orientation observed. Under the condition of furnace cooling, the average grain size is ~30 μm.

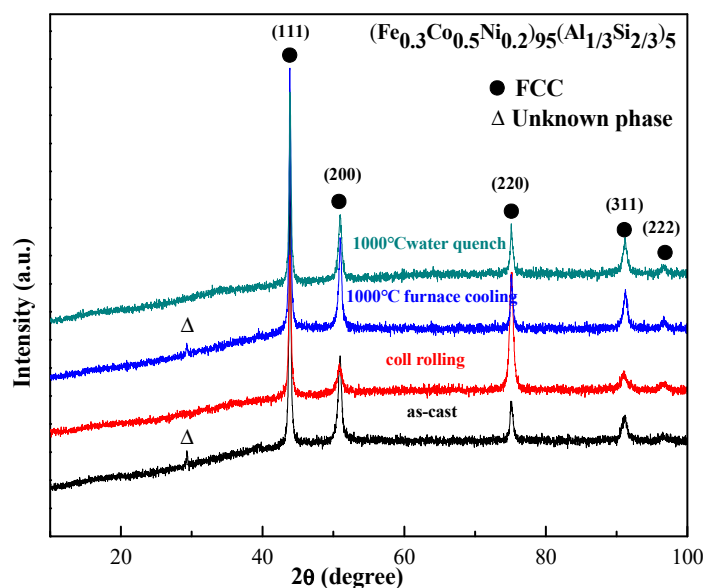**Figure 7.** XRD spectra of the $(Fe_{0.3}Co_{0.5}Ni_{0.2})_{95}(Al_{1/3}Si_{2/3})_5$ alloy produced using maglev melting at different states: As-cast, cold rolling, and annealing at 1000 °C followed by furnace cooling or water quenching.
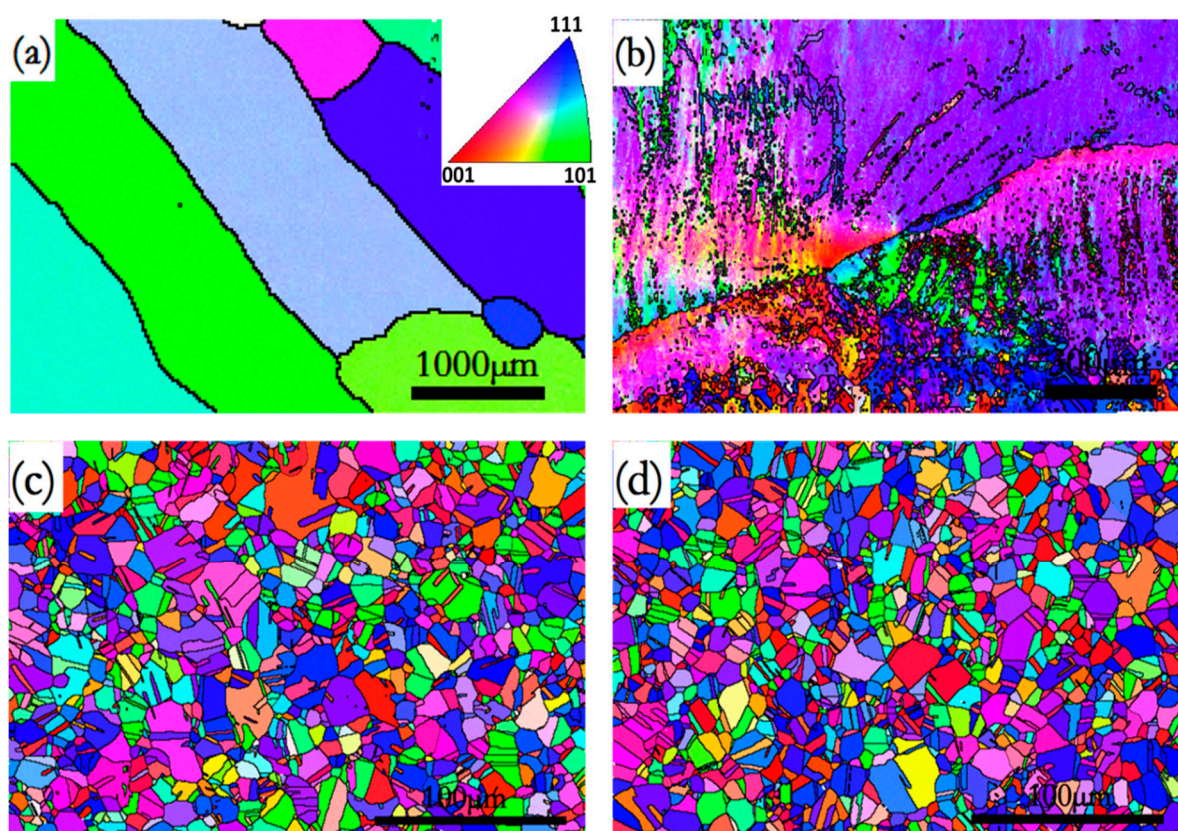

Figure 8. Electron backscatter diffraction (EBSD) images of the $(Fe_{0.3}Co_{0.5}Ni_{0.2})_{95}(Al_{1/3}Si_{2/3})_5$ alloy: (**a**) as-cast, (**b**) cold rolling, (**c**) water quenching, and (**d**) furnace cooling after annealing at 1000 °C.

Figure 9 shows the annular samples of the $(Fe_{0.3}Co_{0.5}Ni_{0.2})_{95}(Al_{1/3}Si_{2/3})_5$ alloy for magnetic induction-coercivity (B-H) measurement. Figure 10 shows the B-H and magnetization-coercivity (M-H) curves of the alloy in the states of as-cast (magnetic suspension melting), cold-rolled, water cooling,

and furnace cooling after heat treatment, respectively. The soft magnetic properties of the alloy in the cold rolled variant are the worst. After the annealing treatment, the coercivity decreased from 510 A/m to 130 A/m due to internal stress release, and the saturation magnetic induction (Bs) improved from 1.14 T to 1.58 T. However, the saturation magnetization is almost constant under cold rolling and heat treatment conditions, which is about 1.49 T. Note that the coercivity of the alloy under vacuum magnetic suspension melting (96 A/m) is significantly lower than that of arc melting (>1000 A/m). The vacuum magnetic suspension melting method is cleaner than arc melting, and causes less oxide inclusions or other impurity in the ingot, and hence introduces much fewer magnetic domain pinning points in the alloy, leading to lower coercivity.

Figure 11 shows the hysteresis loss curve of the $(Fe_{0.3}Co_{0.5}Ni_{0.2})_{95}(Al_{1/3}Si_{2/3})_5$ alloy in different states. Under the power frequency conditions (50 Hz 1 T), the hysteresis loss (Ps) of the alloy in the states of as-cast, cold-rolled, water cooling, and furnace cooling after annealing is 3.13 W/kg, 8.91 W/kg, 4.26 W/kg, and 4.43 W/kg, respectively. In the application of soft magnetic materials, hysteresis loss energy will convert into heat, which will increase the temperature of the equipment and reduce working efficiency. Therefore, the hysteresis loss should be kept as small as possible.

Figure 12 presents the room temperature tensile stress-strain curves of the $(Fe_{0.3}Co_{0.5}Ni_{0.2})_{95}(Al_{1/3}Si_{2/3})_5$ alloy in the as-cast, cold-rolled, and annealed states. The specific values are listed in the Table 2. It shows that the as-cast alloy has the lowest strength, but with satisfactory ductility up to 25% elongation at room temperature. For the cold-rolled alloy, it has the lowest elongation of 1.3% but the highest yield and fracture stresses due to the work hardening.

Table 2. The magnetic properties and tensile behavior of $(Fe_{0.3}Co_{0.5}Ni_{0.2})_{95}(Al_{1/3}Si_{2/3})_5$ in different states.

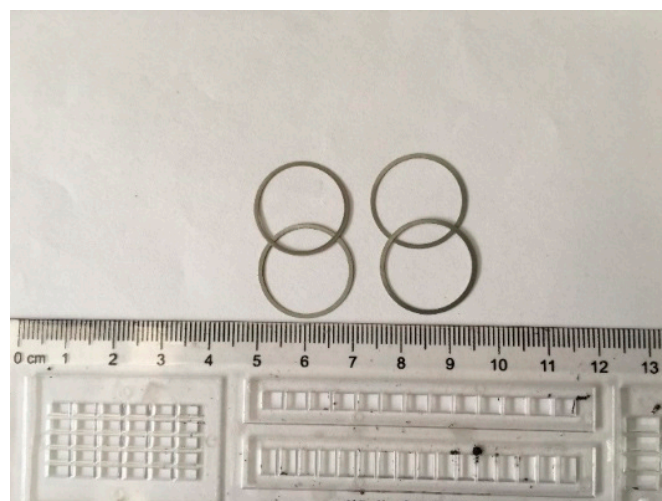| $(Fe_{0.3}Co_{0.5}Ni_{0.2})_{95}(Al_{1/3}Si_{2/3})_5$	Hc (A/m)	Ms (T)	$\sigma_{0.2}$ (MPa)	σ_{max} (MPa)	ε_p (%)
Magnetic levitation melting	96	1.49	176.1	402.4	26.8
Cold rolling	510	1.48	779.6	917.7	1.3
Water quenching	130	1.40	261.5	558.3	38.3
Furnace cooling	165	1.47	235.5	572.4	33.2

Figure 9. The annular samples that were machined for magnetic induction-coercivity (B-H) measurements: Inner diameter is 18 mm, outer diameter is 20 mm, and thickness is 0.3 mm.
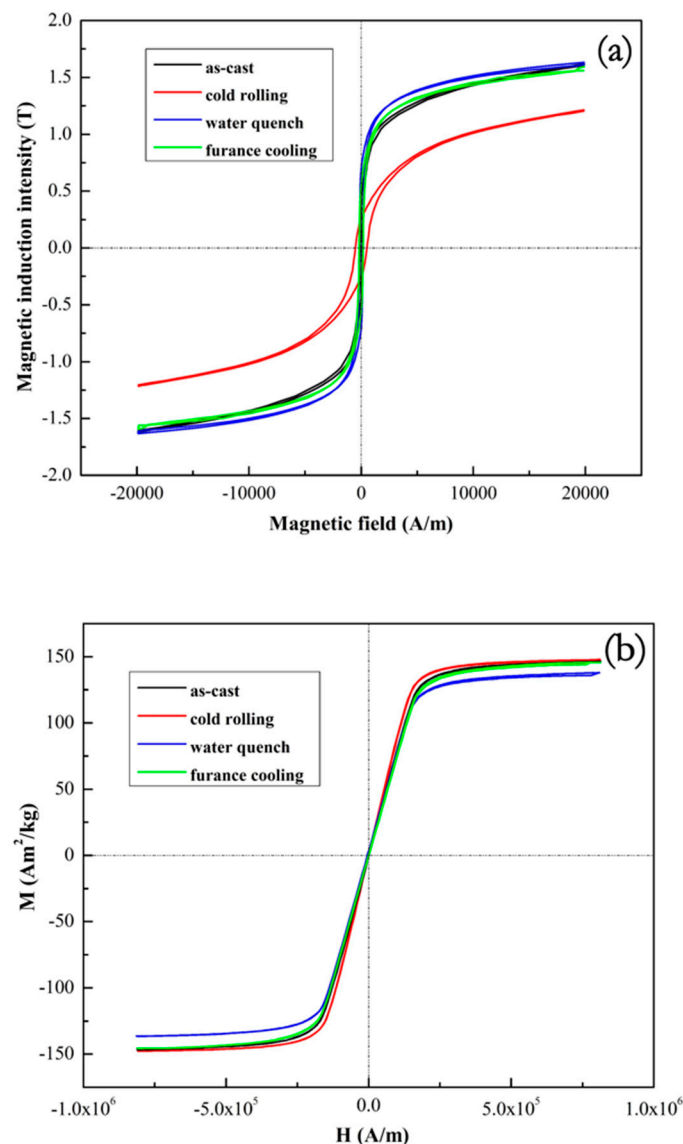
Figure 10. (**a**) magnetic induction-coercivity (B-H) and (**b**) magnetization-coercivity (M-H) (sample size: $1 \times 1 \times 4$ mm^3) curves of $(Fe_{0.3}Co_{0.5}Ni_{0.2})_{95}(Al_{1/3}Si_{2/3})_5$ alloys in the as-cast, cold rolling, and annealed states.

Magnetic materials have been developed for decades. As is well known, silicon steel is most widely used as soft magnetic material at relatively low price. However, the complex production process and large energy consumption restrict its application range [43]. New materials, such as amorphous and nanocrystalline soft magnetic materials, also have excellent soft magnetic properties, but their applications are limited by their poor mechanical properties and thermal stability. In contrast, the high entropy soft magnetic material such as $(Fe_{0.3}Co_{0.5}Ni_{0.2})_{95}(Al_{1/3}Si_{2/3})_5$ as identified in the present study can make up for the deficiency of silicon steel and amorphous soft magnetic material. It has simple preparation process and stable crystal structure, and it also has balanced magentic and mechanical properties. It can be seen from Figure 13, the $(Fe_{0.3}Co_{0.5}Ni_{0.2})_{95}(Al_{1/3}Si_{2/3})_5$ alloy reported in this study (marked by the star) presents better magnetic properties than other soft magnetic high entropy alloys.
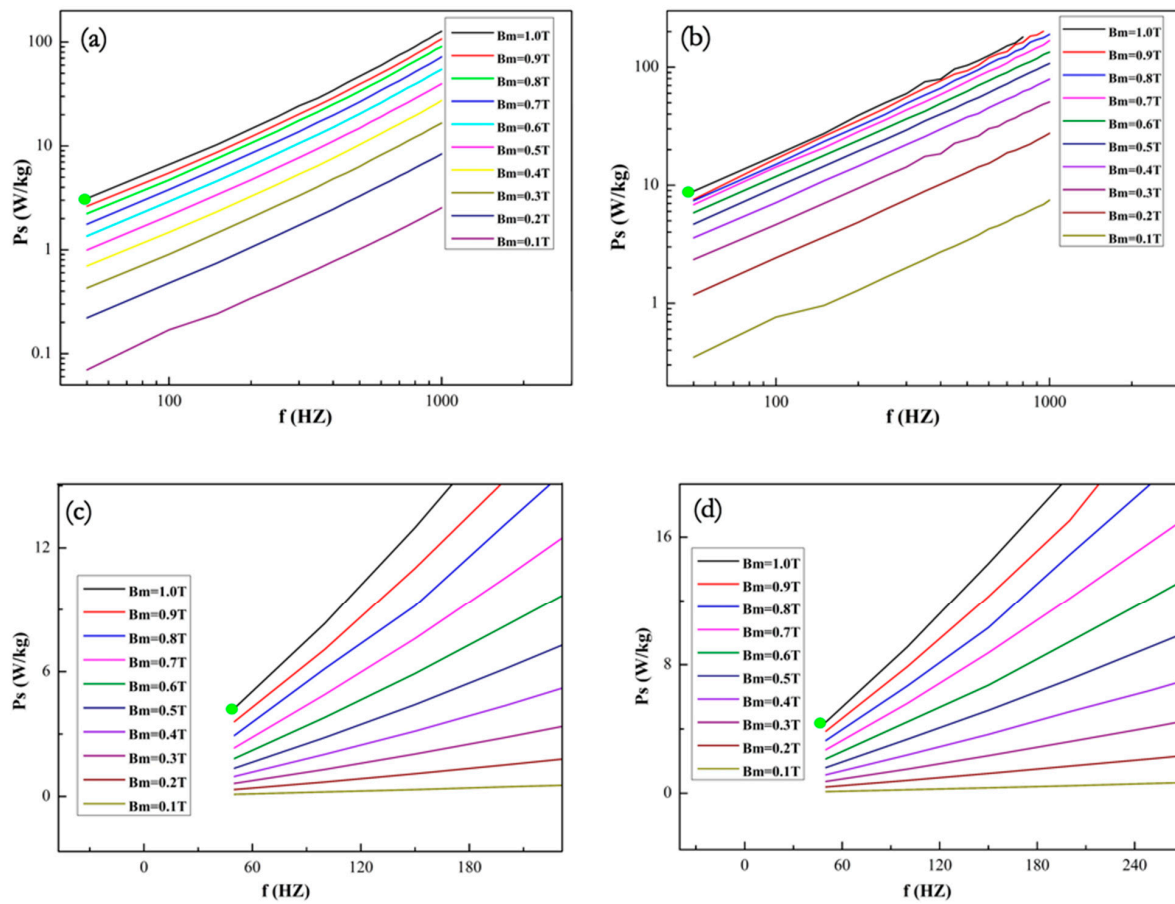
Figure 11. Power loss curves of the $(Fe_{0.3}Co_{0.5}Ni_{0.2})_{95}(Al_{1/3}Si_{2/3})_5$ alloy: (**a**) as-cast, (**b**) cold rolled, (**c**) water quenching, and (**d**) furnace cooling after annealing at 1000 °C.
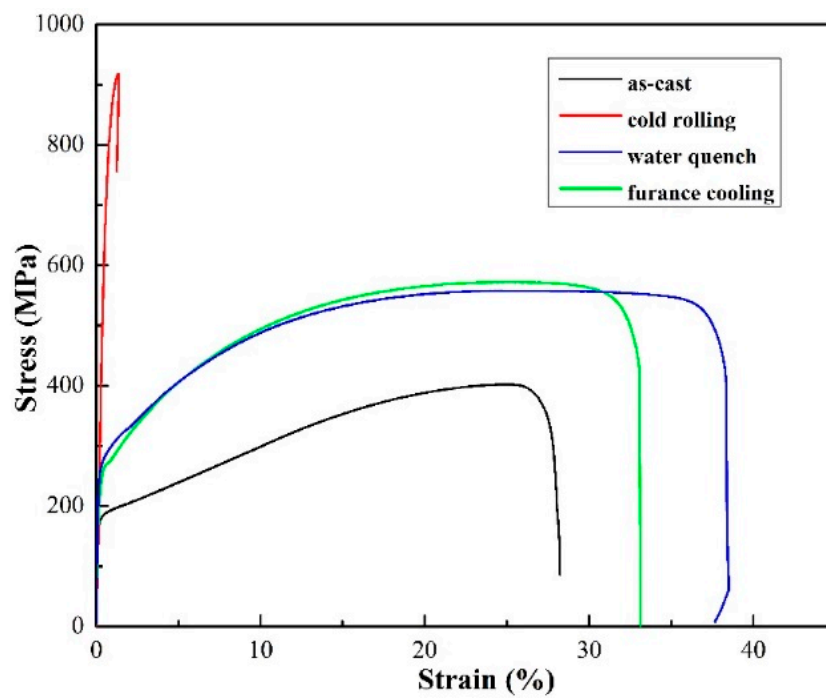

Figure 12. Tensile stress-strain curves of the $(Fe_{0.3}Co_{0.5}Ni_{0.2})_{95}(Al_{1/3}Si_{2/3})_5$ alloys in the as-cast, cold rolling and annealed states.
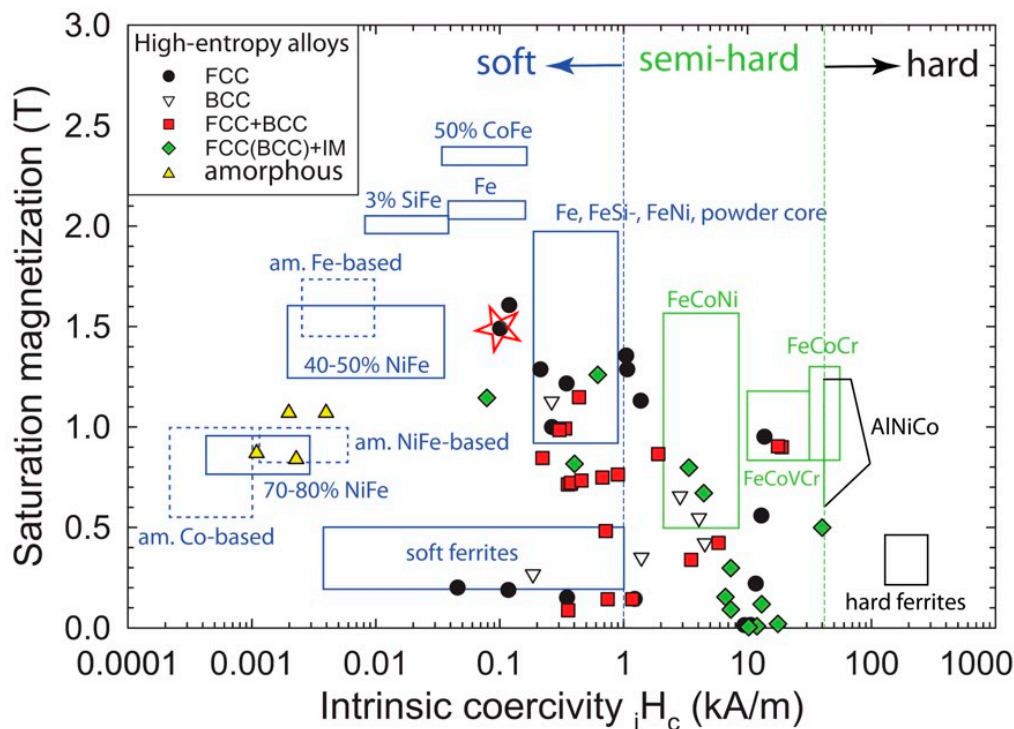
Figure 13. The saturation magnetization and intrinsic coercivity of the $((Fe_{0.3}Co_{0.5}Ni_{0.2})_{95}(Al_{1/3}Si_{2/3})_5$ alloy (marked by the red star) compared with other HEAs, amorphous metals and commercialized soft magnets compiled by Gao et al. Reproduced from [40] with permission of Cambridge University Press.

The relationship between magnetostrictive coefficient and coercivity of alloys for amorphous metals and HEAs reported in the literature is presented in Figure 14. This relationship indicates that identifying alloys with minimum saturation magnetostriction coefficient while optimizing the processing to lower coercivity is very important in developing soft magnetic materials.
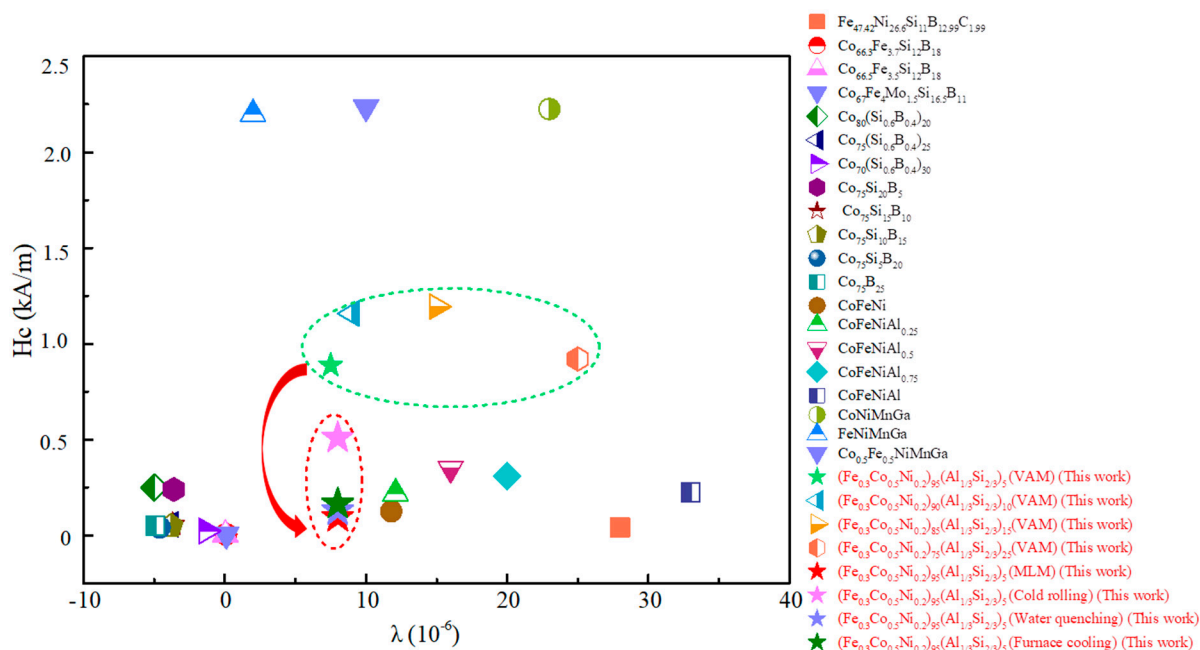

Figure 14. The relationship between saturation magnetostrictive coefficient and coercivity of amorphous alloys and HEAs (data from [46,47,49–52]).

4. Conclusions

Aiming to develop high-performance soft magnets, the magnetic and mechanical properties of a series of $(Fe_{0.3}Co_{0.5}Ni_{0.2})_{100-X}(Al_{1/3}Si_{2/3})_X$ high-entropy alloys (X = 0, 5, 10, 15, and 25) were systematically investigated in this study. The main conclusions are drawn as follows:

(1) The $Fe_{0.3}Co_{0.5}Ni_{0.2}$ base alloy was chosen since it has very small saturation magnetostriction coefficient.

(2) The alloys in the as-cast state maintain an FCC solid solution structure when X $\leq$ 10. More addition of $Al_{1/3}Si_{2/3}$ causes formation of BCC phase. The overall trend is that increasing $Al_{1/3}Si_{2/3}$ contents increases the strength of the alloy at the cost of reduced ductility.

(3) The $(Fe_{0.3}Co_{0.5}Ni_{0.2})_{95}(Al_{1/3}Si_{2/3})_5$ alloy was prepared via maglev melting and then underwent cold-rolling and subsequent heat treatment. The alloy shows high saturation magnetic induction and saturation magnetization. The lower coercive force (about 100 A/m) is found in as-cast and annealed states. The hysteresis loss at low power frequency is about 3-4.5 W/kg.

(4) The $(Fe_{0.3}Co_{0.5}Ni_{0.2})_{95}(Al_{1/3}Si_{2/3})_5$ alloy in the as-cast and after annealing exhibits considerable deformation ability (ductility up to 25% and 38% elongation, respectively) at room temperature.

(5) The $(Fe_{0.3}Co_{0.5}Ni_{0.2})_{95}(Al_{1/3}Si_{2/3})_5$ alloy shows high saturation magnetic induction intensity, low coercivity, and excellent ductility. Hence, it holds good potential as next-generation high-performance soft magnetic materials for wide ranges of energy-saving applications.

Author Contributions: Conceptualization, Y.Z. and T.S.; methodology, M.Z.; formal analysis, T.Z. and D.L.; investigation, M.Z., K.Z., and B.S.; data curation, M.C.G.; writing—original draft preparation, Y.Z., M.Z., and D.L.; writing—review and editing, Y.Z., D.L., and T.S.; supervision, Y.Z.; project administration, Y.Z.

Conflicts of Interest: The authors declare no conflict of interest.

References

1. Yeh, J.-W. Recent progress in high-entropy alloys. *Ann. Chim. Sci. Mat.* **2006**, *31*, 633–648. [CrossRef]
2. Zhang, Y.; Zuo, T.T.; Tang, Z.; Gao, M.C.; Dahmen, K.A.; Liaw, P.K.; Lu, Z.P. Microstructures and properties of high-entropy alloys. *Prog. Mater Sci.* **2014**, *61*, 1–93. [CrossRef]
3. Miracle, D.B.; Senkov, O.N. A critical review of high entropy alloys and related concepts. *Acta Mater* **2017**, *122*, 448–511. [CrossRef]
4. Lu, Z.P.; Wang, H.; Chen, M.W.; Baker, I.; Yeh, J.W.; Liu, C.T.; Nieh, T.G. An assessment on the future development of high-entropy alloys: summary from a recent workshop. *Intermetallics* **2015**, *66*, 67–76. [CrossRef]
5. Lu, Y.; Dong, Y.; Guo, S.; Jiang, L.; Kang, H.; Wang, T.; Wen, B.; Wang, Z.; Jie, J.; Cao, Z.; et al. A promising new class of high-temperature alloys: eutectic high-entropy alloys. *Sci. Rep.* **2014**, *4*, 6200. [CrossRef]
6. Lilensten, L.; Couzinié, J.P.; Perrière, L.; Bourgon, J.; Emery, N.; Guillot, I. New structure in refractory high-entropy alloys. *Mater. Lett.* **2014**, *132*, 123–125. [CrossRef]
7. Tsai, M.-H.; Yeh, J.-W. High-entropy alloys: a critical review. *Mate. Res. Lett.* **2014**, *2*, 107–123. [CrossRef]
8. Tasan, C.C.; Diehl, M.; Yan, D.; Bechtold, M.; Roters, F.; Schemmann, L.; Zheng, C.; Peranio, N.; Ponge, D.; Koyama, M.; Tsuzaki, K.; Raabe, D. An overview of dual-phase steels: advances in microstructure-oriented processing and micromechanically guided design. *Annu. Rev. Mater. Res.* **2015**, *45*, 391–431. [CrossRef]
9. Lyu, Z.; Lee, C.; Wang, S.-Y.; Fan, X.; Yeh, J.-W.; Liaw, P.K. Effects of constituent elements and fabrication methods on mechanical behavior of high-entropy alloys: A review. *Metall. Mater. Trans. A* **2019**, *50*, 1–28. [CrossRef]
10. Gao, M.C.; Yeh, J.-W.; Liaw, P.K.; Zhang, Y. *High-Entropy Alloys*; Springer: Berlin, Germany, 2016.

11. Luo, H.; Li, Z.; Lu, W.; Ponge, D.; Raabe, D. Hydrogen embrittlement of an interstitial equimolar high-entropy alloy. *Corros. Sci.* **2018**, *136*, 403–408. [CrossRef]

12. Shun, T.-T.; Du, Y.-C. Microstructure and tensile behaviors of fcc Al0.3cocrfeni high entropy alloy. *J. Alloys Compd.* **2009**, *479*, 157–160. [CrossRef]

13. Basu, S.; Li, Z.; Pradeep, K.G.; Raabe, D. Strain rate sensitivity of a trip-assisted dual-phase high-entropy alloy. *Front. Mater. Struct. Mater.* **2018**, *5*, 1–10. [CrossRef]

14. Gu, J.; Song, M. Annealing-induced abnormal hardening in a cold rolled crmnfeconi high entropy alloy. *Scr. Mater.* **2019**, *162*, 345–349. [CrossRef]

15. Li, D.; Li, C.; Feng, T.; Zhang, Y.; Sha, G.; Lewandowski, J.J.; Liaw, P.K.; Zhang, Y. High-entropy Al 0.3 cocrfeni alloy fibers with high tensile strength and ductility at ambient and cryogenic temperatures. *Acta Mater.* **2017**, *123*, 285–294. [CrossRef]

16. Feuerbacher, M.; Lienig, T.; Thomas, C. A single-phase bcc high-entropy alloy in the refractory Zr-Nb-Ti-V-Hf system. *Scr. Mater.* **2018**, *152*, 40–43. [CrossRef]

17. Yang, T.; Zhao, Y.L.; Tong, Y.; Jiao, Z.B.; Wei, J.; Cai, J.X.; Han, X.D.; Chen, D.; Hu, A.; Kai, J.J. Multicomponent intermetallic nanoparticles and superb mechanical behaviors of complex alloys. *Science* **2018**, *362*, 933–937. [CrossRef]

18. Zhao, Y.J.; Qiao, J.W.; Ma, S.G.; Gao, M.C.; Yang, H.J.; Chen, M.W.; Zhang, Y. A hexagonal close-packed high-entropy alloy: the effect of entropy. *Mater. Des.* **2016**, *96*, 10–15. [CrossRef]

19. Lu, L.; Chen, X.; Huang, X.; Lu, K. Revealing the maximum strength in nanotwinned copper. *Science* **2009**, *323*, 607–610. [CrossRef]

20. Gao, M.C.; Zhang, B.; Guo, S.M.; Qiao, J.W.; Hawk, J.A. High-entropy alloys in hexagonal close-packed structure. *Metall. Mater. Trans. A* **2016**, *47*, 3322–3332. [CrossRef]

21. Nagase, T.; Takeuchi, A.; Amiya, K.; Egami, T. Solid state amorphization of metastable $Al_{0.5}TiZrPdCuNi$ high entropy alloy investigated by high voltage electron microscopy. *Mater. Chem. Phys.* **2018**, *210*, 291–300. [CrossRef]

22. Huang, H.; Wu, Y.; He, J.; Wang, H.; Liu, X.; An, K.; Wu, W.; Lu, Z. Phase-transformation ductilization of brittle high-entropy alloys via metastability engineering. *Adv. Mater.* **2017**, *29*, 1701678. [CrossRef]

23. Li, Z.; Tasan, C.C.; Pradeep, K.G.; Raabe, D. A trip-assisted dual-phase high-entropy alloy: grain size and phase fraction effects on deformation behavior. *Acta Mater.* **2017**, *131*, 323–335. [CrossRef]

24. Senkov, O.N.; Wilks, G.B.; Miracle, D.B.; Chuang, C.P.; Liaw, P.K. Refractory high-entropy alloys. *Intermetallics* **2010**, *18*, 1758–1765. [CrossRef]

25. Miracle, D.; Miller, J.; Senkov, O.; Woodward, C.; Uchic, M.; Tiley, J. Exploration and development of high entropy alloys for structural applications. *Entropy* **2014**, *16*, 494–525. [CrossRef]

26. Tong, Y.; Chen, D.; Han, B.; Wang, J.; Feng, R.; Yang, T.; Zhao, C.; Zhao, Y.L.; Guo, W.; Shimizu, Y. Outstanding tensile properties of a precipitation-strengthened FeCoNiCrTi0.2 high-entropy alloy at room and cryogenic temperatures. *Acta Mater.* **2019**, *165*, 228–240. [CrossRef]

27. Sun, S.J.; Tian, Y.Z.; Lin, H.R.; Yang, H.J.; Dong, X.G.; Wang, Y.H.; Zhang, Z.F. Achieving high ductility in the 1.7 GPa grade cocrfemnni high-entropy alloy at 77 K. *Mater. Sci. Eng. A* **2019**, *740–741*, 336–341. [CrossRef]

28. Liu, K.; Komarasamy, M.; Gwalani, B.; Shukla, S.; Mishra, R.S. Fatigue behavior of ultrafine grained triplex $Al_{0.3}CoCrFeNi$ high entropy alloy. *Scr. Mater.* **2019**, *158*, 116–120. [CrossRef]

29. Gwalani, B.; Gorsse, S.; Choudhuri, D.; Zheng, Y.; Mishra, R.S.; Banerjee, R. Tensile yield strength of a single bulk $Al_{0.3}CoCrFeNi$ high entropy alloy can be tuned from 160 MPa to 1800 MPa. *Scr. Mater.* **2019**, *162*, 18–23. [CrossRef]

30. Couzinié, J.P.; Dirras, G. Body-centered cubic high-entropy alloys: from processing to underlying deformation mechanisms. *Mater. Charact.* **2019**, *147*, 533–544. [CrossRef]

31. Li, D.; Gao, M.C.; Hawk, J.A.; Zhang, Y. Annealing effect for the $Al_{0.3}CoCrFeNi$ high-entropy alloy fibers. *J. Alloys Compd.* **2019**, *778*, 23–29. [CrossRef]

32. Zuo, T.; Gao, M.C.; Ouyang, L.; Yang, X.; Cheng, Y.; Feng, R.; Chen, S.; Liaw, P.K.; Hawk, J.A.; Zhang, Y. Tailoring magnetic behavior of $CoFeMnNi_x$ (X = Al, Cr, Ga, and Sn) high entropy alloys by metal doping. *Acta Mater.* **2017**, *130*, 10–18. [CrossRef]

33. Zuo, T.; Yang, X.; Liaw, P.K.; Zhang, Y. Influence of bridgman solidification on microstructures and magnetic behaviors of a non-equiatomic FeCoNiAlSi high-entropy alloy. *Intermetallics* **2015**, *67*, 171–176. [CrossRef]

34. Zhang, Y.; Zuo, T.; Cheng, Y.; Liaw, P.K. High-entropy alloys with high saturation magnetization, electrical resistivity, and malleability. *Sci. Rep.* **2013**, *3*, 1455. [CrossRef] [PubMed]

35. Lucas, M.S.; Mauger, L.; Munoz, J.A.; Xiao, Y.; Sheets, A.O.; Semiatin, S.L.; Horwath, J.; Turgut, Z. Magnetic and vibrational properties of high-entropy alloys. *J. Appl. Phys.* **2011**, *109*, 07E307. [CrossRef]

36. Singh, S.; Wanderka, N.; Kiefer, K.; Siemensmeyer, K.; Banhart, J. Effect of decomposition of the Cr–Fe–Co rich phase of alcocrcufeni high entropy alloy on magnetic properties. *Ultramicroscopy* **2011**, *111*, 619–622. [CrossRef] [PubMed]

37. Hu, F.-X.; Shen, B.-G.; Sun, J.-R. Magnetic entropy change in $Ni_{51.5}Mn_{22.7}Ga_{25.8}$ alloy. *Appl. Phys. Lett.* **2000**, *76*, 3460–3462. [CrossRef]

38. Lucas, M.S.; Belyea, D.; Bauer, C.; Bryant, N.; Michel, E.; Turgut, Z.; Leontsev, S.O.; Horwath, J.; Semiatin, S.L.; Mchenry, M.E. Thermomagnetic analysis of fecocr X Ni alloys: magnetic entropy of high-entropy alloys. *J. Appl. Phys.* **2013**, *113*, 17A923. [CrossRef]

39. Madni, A.M.; Ross, A. Exploring concept trade-offs. In *Using Tradeoff Analyses to Identify Value and Risk*; Wiley: New York, NY, USA, 2016.

40. Gao, M.C.; Miracle, D.B.; Maurice, D.; Yan, X.; Zhang, Y.; Hawk, J.A. High-Entropy functional materials. *J. Mater. Res.* **2018**, *33*, 3138–3155. [CrossRef]

41. Gutfleisch, O.; Willard, M.A.; Brück, E.; Chen, C.H.; Sankar, S.G.; Liu, J.P. Magnetic materials and devices for the 21st century: stronger, lighter, and more energy efficient. *Adv. Mater.* **2011**, *23*, 821–842. [CrossRef]

42. Garibaldi, M.; Ashcroft, I.; Simonelli, M.; Hague, R. Metallurgy of high-silicon steel parts produced using selective laser melting. *Acta Mater.* **2016**, *110*, 207–216. [CrossRef]

43. Krings, A.; Boglietti, A.; Cavagnino, A.; Sprague, S. Soft magnetic material status and trends in electric machines. *IEEE Trans. Ind. Electron.* **2017**, *64*, 2405–2414. [CrossRef]

44. Kruzic, J.J. Bulk metallic glasses as structural materials: A review. *Adv. Eng. Mater.* **2016**, *18*, 1308–1331. [CrossRef]

45. Da Silveira, G.; Slack, N. Exploring the trade-off concept. *Inter. J. Oper. Prod. Manage.* **2001**, *21*, 949–964. [CrossRef]

46. Zuo, T.T.; Li, R.B.; Ren, X.J.; Zhang, Y. Effects of Al and Si addition on the structure and properties of CoFeNi equal atomic ratio alloy. *J. Magn. Magn. Mater.* **2014**, *371*, 60–68. [CrossRef]

47. Zhang, M. Soft magnetic properties of $(Fe_{0.3}Co_{0.5}Ni_{0.2})$ 100-X $(Al_{1/3}Si_{2/3})$ X high-entropy alloy. Master's Thesis, University of Science and Technology Beijing, Beijing, China, 1 January 2019.

48. Tang, Z.; Gao, M.C.; Diao, H.; Yang, T.; Liu, J.; Zuo, T.; Zhang, Y.; Lu, Z.; Cheng, Y.; Zhang, Y. Aluminum alloying effects on lattice types, microstructures, and mechanical behavior of high-entropy alloys systems. *JOM* **2013**, *65*, 1848–1858. [CrossRef]

49. Vasquez, M.; Ascasibar, E.; Hernando, A.; Nielsen, O.V. Co-Si-B and Fe-Co-B amorphous alloys: induced anisotropy and various magnetic properties. *J. Magn. Magn. Mater.* **1987**, *66*, 37–44. [CrossRef]

50. Hernando, B.; Sanchez, M.L.; Prida, V.M.; Tejedor, M.; Vázquez, M. Magnetoimpedance effect in amorphous and nanocrystalline ribbons. *J. Appl. Phys.* **2001**, *90*, 4783–4790. [CrossRef]

51. Caltun, O.; Rao, G.S.N.; Rao, K.H.; Parvatheeswara Rao, B.; Dumitru, I.; Kim, C.-O.; Kim, C. The influence of Mn doping level on magnetostriction coefficient of cobalt ferrite. *J. Magn. Magn. Mater.* **2007**, *316*, e618–e620. [CrossRef]

52. Zhukov, A.; Churyukanova, M.; Kaloshkin, S.; Semenkova, V.; Gudoshnikov, S.; Ipatov, M.; Talaat, A.; Blanco, J.M.; Zhukova, V. Effect of annealing on magnetic properties and magnetostriction coefficient of Fe-Ni-based amorphous microwires. *J. Alloys Compd.* **2015**, *651*, 718–723. [CrossRef]